

# High-Resolution Near Infrared Spectroscopy of HD 100546: IV. Orbiting Companion Disappears on Schedule

SEAN D. BRITTAIN,<sup>1,\*</sup> JOAN R. NAJITA,<sup>2</sup> AND JOHN S. CARR<sup>3</sup>

<sup>1</sup>*Clemson University  
118 Kinard Laboratory  
Clemson, SC 29634, USA*

<sup>2</sup>*National Optical Astronomy Observatory  
950. N. Cherry Ave.  
Tucson, AZ 85719, USA*

<sup>3</sup>*Department of Astronomy  
University of Maryland  
College Park, MD 20742, USA*

(Received ...; Revised August 2, 2019; Accepted ...)

Submitted to ApJ

## ABSTRACT

HD 100546 is a Herbig Ae/Be star surrounded by a disk with a large central region that is cleared of gas and dust (i.e., an inner hole). High-resolution near-infrared spectroscopy reveals a rich emission spectrum of fundamental ro-vibrational CO emission lines whose time variable properties point to the presence of an orbiting companion within the hole. The Doppler shift and spectroastrometric signal of the CO  $v=1-0$  P26 line, observed from 2003 to 2013, are consistent with a source of excess CO emission that orbits the star near the inner rim of the disk. The properties of the excess emission are consistent with those of a circumplanetary disk. In this paper, we report follow up observations that confirm our earlier prediction that the orbiting source of excess emission would disappear behind the near side of the inner rim of the outer disk in 2017. We find that while the hotband CO lines remained unchanged in 2017, the  $v=1-0$  P26 line and its spectroastrometric signal returned to the profile observed in 2003. With these new observations, we further constrain the origin of the emission and discuss possible ways of confirming the presence of an orbiting planetary companion in the inner disk.

*Keywords:* stars: circumstellar matter, individual (HD 100546), planets and satellites: formation, protoplanetary disks

## 1. INTRODUCTION

The identification of forming planets will allow us to connect the initial conditions in disks to the kinds of planets that form, connect the initial architecture of planetary systems to the final distribution of planets observed around main sequence stars, and validate indirect signposts of gas giant formation. High-resolution near-infrared spectroscopy of the circumplanetary material surrounding forming gas giant planets will help to elucidate the physics of planet formation. For example,

determining how material accretes from the circumstellar disk to the circumplanetary disk and finally on the planet will shed light on what sets the mass of gas giant planets. Measuring the size and temperature of circumplanetary disks will provide observational constraints on the initial conditions for the *in situ* formation of satellites (e.g., the Galilean moons; Canup & Ward 2002; Ward & Canup 2010).

While even the highest spatial resolution instruments planned for next generation facilities (e.g., the 30-meter class telescopes) will only at best be able to marginally resolve such structures, high-resolution spectroscopy of warm gas using instruments on current 10-meter class telescopes can serve as a surrogate for high-spatial resolution. Spectroastrometric observations reported over

Corresponding author: Sean Brittain  
sbritt@clemson.edu

\* Visiting Scientist, NOAO

the past decade, which provide complementary sub-milliarcsecond-scale spatial information on the dynamics of disk gas, demonstrate the promise of this approach (Pontoppidan et al. 2008, 2011; Brittain et al. 2009, 2013, 2014, 2015).

Theory predicts that an orbiting giant planet will dynamically clear a gap in the vicinity of its orbit, or possibly deplete the entire inner disk creating a large inner hole. The large optically thin region that results will produce a spectral energy distribution (SED) with a large deficit at mid-infrared wavelengths, a transition disk SED. Gas accreting through the disk onto the forming gas giant planet is expected to form a circumplanetary disk that fills roughly 1/3 of the Hill radius (e.g., Quillen & Trilling 1998). Recent modeling indicates that circumplanetary structures are vertically extended and intrinsically 3D, although they retain the rotationally supported disk found in 2D simulations (e.g., Ayliffe & Bate 2009; Machida et al. 2010; Tanigawa et al. 2012; Gressel et al. 2013; Szulágyi et al. 2014).

Although observational evidence of circumplanetary structures remains scant, several recent studies have reported evidence for planetary companions in the cleared inner regions of transition disks. The young stars LkCa 15, PDS 70, and HD 142527 harbor companions (perhaps a stellar companion in the case of HD 142527) that appear to be accreting as evidenced by the H $\alpha$  emission detected from these sources (Sallum et al. 2015; Wagner et al. 2018; Close et al. 2014, respectively). Although attempts to detect a circumplanetary disk with ALMA have yielded little success thus far (e.g., Keppler et al. 2019; Pineda et al. 2019; but see Pérez et al. 2019, high-contrast near-infrared (NIR) imagery of LkCa 15 (Kraus & Ireland 2012; Sallum et al. 2015), and PDS 70 (Keppler et al. 2018; Christiaens et al. 2019) reveal compact NIR emission that could be produced by forming gas giant planets and/or their circumplanetary disk. Complementary information about any circumplanetary emission can be acquired with high-resolution NIR spectroscopy.

We have previously identified in the Herbig Ae/Be system HD 100546 a possible signpost of giant planet formation: an orbiting source of 5 $\mu$ m CO fundamental emission that may arise in a circumplanetary disk (Brittain et al. 2014). Herbig Ae/Be stars are pre- and zero-age main sequence stars with accretion disks (e.g., Waters & Waelkens 1998). The disk orbiting HD 100546 is devoid of dust interior to  $R_{\text{hole}} = 15.7 \pm 0.8$  au (Jamilahmadi et al. 2018). This region is also devoid of molecular gas and PAHs (Habart et al. 2006; Brittain et al. 2009; van der Plas et al. 2009; Carmona et al. 2011; Liskowsky et al. 2012)

Using Phoenix on Gemini South and CRIRES on the Very Large Telescope, we inferred the presence of a potential companion within the inner hole, based on an excess component of the high-J  $v=1-0$  ro-vibrational CO emission that varies relative to the stable hotband emission (Brittain et al. 2014). The variation of the Doppler shift and the spectroastrometric signal of the excess component over a 10 year period can be explained by a compact source of emission in a Keplerian orbit near the edge of the disk gap (Fig. 1). The discovery of a companion at the location inferred for the orbiting component has been reported based on high contrast near-infrared imaging (Currie et al. 2015).

The CO flux of the excess component is consistent with emission from a circumplanetary disk with a radius of  $\sim 0.3$  AU if we assume the emitting gas is optically thick and at the same temperature as the circumstellar gas near the disk edge (1400 K; Brittain et al. 2013). These values are consistent with the theoretically predicted thermal properties of circumplanetary disks of giant planets. Szulágyi et al. (2014) reported a disk temperature of  $\sim 2000$ K out to a Hill radius  $R_{\text{Hill}} \sim 0.8$  au for the case, in their theoretical study, of a 10  $M_{\text{J}}$  planet at 5 au (see also Szulágyi 2017; Szulágyi & Mordasini 2017). Similar temperatures have been reported for the inner circumplanetary disk in other three-dimensional radiation hydrodynamical simulations (Klahr & Kley 2006; Gressel et al. 2013).

From our earlier observations, we constrained the orbital radius of the excess CO emission source to  $R=12.9_{-1.3}^{+1.5}$  au. We were also able to constrain the 2003 orbital phase relative to the northwest extent of the semi-major axis to  $\phi=6_{-20}^{+15}$ ° (Brittain et al. 2014). Based on this orbit, we predicted that the compact emission source would disappear behind the near side of the inner disk wall sometime between February 2017 and February 2019. Here we report follow-up spectroscopy of HD 100546 acquired in July 2017 and December 2017. We show that the excess emission component is no longer evident, with the profile of the  $v=1-0$  lines having returned to the line shape originally observed in 2003.

## 2. OBSERVATIONS

We acquired high-resolution ( $R=50,000$ ), near-infrared spectra of HD 100546 on July 9, 2017 and December 3-4, 2017 using PHOENIX at the Gemini South telescope (Hinkle et al. 2003, 2000, 1998). In addition the hot star HIP 60718 was observed for telluric correction. The 4 pixel slit ( $0''.34$ ) was used for all observations providing 1.5 km s $^{-1}$  per pixel sampling of the spectrum. The seeing in the  $M$ -band during these epochs ranged from

0".9–1.0" and the airmass of the observations ranged from 1.5–1.6. In July, half of the spectra were taken with the slit in its default position angle of 90° east of north, and the other half were taken with the slit rotated 180°. In the December, all of the spectra were acquired with the slit in its default position. A summary of observations is presented in Table 1.

Observations were centered near 2034 cm<sup>-1</sup>, which covers the v=1-0 P26 line (hereafter we will refer to this transition as P26) and numerous hot band lines. These same transitions were also observed in 2003, 2006, 2010, and 2013. These spectra were previously presented in Brittain et al. (2014).

Observations in the *M*-band are dominated by a strong thermal background. Therefore, an ABBA nod pattern between two positions separated by  $\sim 5''$  is used to cancel the thermal continuum to first order. The scans are flat fielded, cleaned of hot and dead pixels, including cosmic ray hits, and then combined in the sequence (A<sub>1</sub>-B<sub>1</sub>-B<sub>2</sub>+A<sub>2</sub>)/2. Because the spectra are curved along the detector, they are first rectified by finding the centroid of the point spread function (PSF) in each column. A third degree polynomial was fit to the centroids and used to determine the shift of each column to a common row.

In principle, the spectra can also be tilted along the slit. To check this, we compared the sky emission spectrum at the bottom of the slit to the spectrum at the top of the slit. The offset was less than half of a pixel along the length of the slit. A sky emission spectrum generated by the Spectral Synthesis Program (Kunde & Maguire 1974), which accesses the 2000HITRAN molecular database (Rothman et al. 2003) was used to measure the shift of each row. A first degree polynomial was fit to the central wavenumber of each row to measure the shift. Each row was then rectified in the spectral direction.

To capture all of the CO emission, a 2" window was extracted to generate the one-dimensional spectrum. The wavelength calibration was achieved by fitting an atmospheric transmittance model generated by the Spectral Synthesis Program. Each spectrum is then ratioed to a standard star observed at a similar airmass to remove telluric absorption lines. Areas where the transmittance is below 50% are omitted (Figs. 2a & 2b).

The spectra acquired in July were observed with two PAs in order to make a spectroastrometric measurement of the emission lines (see for example, Brittain et al. 2015, 2018). To measure the spectroastrometric signal of the emission lines, the centroids of the A and B rows of the rectified array are measured for each column and then averaged. The centroid measurements of the paral-

lel and anti-parallel position angles are then subtracted and divided by two in order to remove systematic features. The spectroastrometric measurement is presented in figure 3.

### 3. RESULTS

To check for variability of the CO emission (due to artifacts and/or intrinsic variation), we averaged together six hotband CO lines that were not blended or significantly impacted by telluric absorption (Table 2). As in previous analyses, the spectra were rescaled so that the equivalent widths of the hotband lines were the same from epoch to epoch (Brittain et al. 2013, 2014). We then differenced the averaged profile from each epoch with the averaged profile from 2003 (Fig. 4). No significant variability in the shape of the lines is detected relative to 2003 in any of the epochs.

A similar analysis was performed for the v=1-0 P26 CO line. The equivalent widths of the P26 line from each epoch were scaled with the value used to scale the hotband lines from their respective epoch. As noted in previous papers (Brittain et al. 2009, 2014, 2015), the P26 line was substantially different both in flux and shape in 2006, 2010, and 2013 relative to 2003. We have two epochs in 2017. In neither epoch is the residual of the difference between the 2003 and 2017 epochs above the 1 $\sigma$  level (Fig. 5). While the signal-to-noise of the spectroastrometric measurement is low due to the poor seeing at the time of the observation, the signal of the P26 lines is observed and consistent with gas orbiting in an axisymmetric disk (Fig. 3).

Over time, the v=1-0 P26 line has varied relative to the hotband lines. Because these lines are observed simultaneously in the same spectrum, we are confident that the variability of the v=1-0 line is intrinsic to the source of emission rather than an artifact such as misalignment of the slit with the PSF of the source (e.g., Hein Bertelsen et al. 2014).

It is now evident that the excess CO emission was visible for fewer than 14.5 yrs, so the upper limit on the period of the orbit is 29yrs. This allows us to refine the orbital parameters of the source of emission. Assuming a stellar mass of 2.2M<sub>⊙</sub> (Pineda et al. 2019) the object must be orbiting within 12.3 au (Fig. 6). Adopting the disk inclination measured with mid-infrared interferometry (47°; Jamialahmadi et al. 2018), we also constrain the orbital phase to  $\phi = -5.5^\circ - +8.7^\circ$  and the inner extent of the CO emission to >11.6 au. Thus the orbital radius of this source of emission is constrained to 11.6 au – 12.3 au. Recent ALMA measurements provide a slightly different measurement of the stellar mass (2.05±0.01 M<sub>⊙</sub>) and disk inclination (40.1° ± 0.1°;

Casassus & Perez 2019). These values shift the center of the contours to 11.5 au and  $-2^\circ$  so that the constraint on the orbital phase is  $\phi = -22^\circ - +15^\circ$  and the orbital radius is constrained to 10.5 au – 12.3 au. This is interior to the inner edge of the outer disk inferred from mid-infrared interferometry (15.7 au Jami-  
alahmadi et al. 2018) and NIR high contrast imagery (Follette et al. 2017). The separation we infer is independent of the distance to the source as it is inferred from the velocity and period of the orbit, so it should not be rescaled with the updated distance to HD 100546 available from GAIA (cf., Follette et al. 2017; Jamialahmadi et al. 2018).

#### 4. DISCUSSION

A decade and a half of high resolution CO spectroscopy of HD 100546 provides strong evidence for an orbiting source of CO emission that has the temperature and emitting area expected for a circumplanetary disk. Some recent publications (Follette et al. 2017; Pineda et al. 2019) have been dismissive of the CO spectroastrometric results, by making incorrect reference to Fedele et al. (2015), whose criticism was directed at the line profile of the ro-vibrational OH lines (see the appendix for further details). While it is true that an offset of the slit from the stellar position can produce an asymmetric spectroastrometric signal and line profile (see Brittain et al. 2015), this cannot explain the CO results for HD 100546. The simple reason is that the  $v=1-0$  and hot-band lines were observed simultaneously, yet they show different spectroastrometric signals and profiles in data from 2006 to 2013.

Even if that were not the case, slit offsets cannot produce the large asymmetries observed, because the slit width in our observations was wider than the size of the inner rim in HD 100546. Modeling of the effects of slit misalignment on observations of axisymmetric disk emission (Brittain et al. 2015) shows that, in this situation, offsets even as large as the full slit width are unable to produce the large asymmetries observed in the CO  $v=1-0$  spectroastrometric signal.

Orbiting sources of emission have also been detected in the inner region of other transition disks, albeit for smaller fractions of their orbits than in the case of HD 100546. As one exciting example, the three emission sources in the LkCa 15 system show consistent orbital motion at  $\sim 19$  au from the star in data taken over more than 6 years (Sallum et al. 2016, 2019 in preparation).

Whether the orbiting source of excess CO emission in the HD 100546 system actually arises in a circumplanetary disk (or, alternatively, in an orbiting hot spot on the disk wall, or another component) is as yet unclear.

Efforts to detect an associated source of continuum emission at  $\sim 12$  au have been inconclusive. The separation at maximum elongation is 100 mas which is very close to the inner working angle of high contrast imagers on 8 m class telescopes (e.g., Follette et al. 2017). Currie et al. (2015) reported the presence of a NIR point source interior to the inner rim in their image of the disk (HD 100546c) at a PA consistent with the inferred orbit of the CO excess emission source. Subsequent GPI imagery of the disk did not confirm this result (Follette et al. 2017); however, it is likely that the emission source fell behind the coronagraphic mask in this epoch (Currie et al. 2017). High contrast imagers that can more easily probe smaller orbital distances (e.g., instruments such as SCExAO on the Subaru Telescope and its successors) can potentially image the source of emission when it emerges from behind the inner rim of the disk in 2031.

If the source of CO excess emission is a circumplanetary disk, it may be detectable in the near-infrared or millimeter dust continuum, depending on its dust-to-gas ratio and other factors. A recent study of the observability of circumplanetary disks with ALMA found that a circumplanetary disk around a 3  $M_J$  planet at 5 au would produce a flux of  $\sim 1$  mJy/beam and be detectable at  $440 \mu\text{m}$  in  $\sim 5$  hr of integration for a system  $\sim 100$  pc away (Szulágyi et al. 2018). In comparison, the ALMA upper limits reported by Pineda et al. (2019) at  $870 \mu\text{m}$  at the position of HD 100546c are 5 times smaller ( $198 \mu\text{Jy}$ ). The theoretical flux estimate assumes a dust-to-gas ratio of 0.01, although as the authors note, the dust-to-gas ratio could be much smaller: the circumplanetary disk is fed by vertical meridional flow from the outer disk, and only the small grains that are well coupled to the gas are entrained in the flow, with larger solids filtered out by the pressure bump of the outer disk. Perhaps the resulting low dust-to-gas ratio of the CPD reduces the submillimeter flux to a level consistent with the ALMA upper limit.

There are additional lines of evidence suggesting that the dust-to-gas ratio of the accreting material in HD 100546 is substantially lower than 0.01. Firstly, the stellar photospheric abundance of refractory material in HD 100546 is depleted relative to volatile elements, a result that led (Kama et al. 2015) to conclude that the dust-to-gas ratio of the accreting material is 0.001. Secondly, Dong et al. (2018) point out that the disk mass of HD 100546 (and other Herbig Ae/Be stars) inferred from its submillimeter continuum emission (i.e., the dust) and the assumption that the dust-to-gas ratio is 0.01 implies that the accretion onto the star can only be maintained for  $\sim 10^5$  yrs - a small fraction of the system age. Thus they conclude that the dust-to-gas

ratio of disks around Herbig Ae/Be stars is substantially lower than 0.01 potentially making it difficult to detect the circumplanetary disk in the submillimeter.

Despite these considerations, Pérez et al. (2019) have reported the possible detection with ALMA of a circumplanetary disk in dust continuum emission and gas kinematics. The continuum emission source, located 51 mas from the star (or 5.6 au adopting a distance of  $110.0 \pm 0.6$  pc from Gaia Collaboration et al. 2018) and at a PA of  $37^\circ$  in September 2017, is closer to the star and at a different PA than the orbiting source of excess CO emission studied here.

How can we confirm the presence of an orbiting giant planetary companion to HD 100546 without waiting for it to emerge from behind the disk in 2031? Perhaps the most promising approach is through the reflex motion the companion induces in the central star. If a 5  $M_J$  companion orbits 12 au from the star, the semi-major axis of the star's orbit is 0.24 mas. Recent studies that have combined the Hipparcos and Gaia DR2 astrometric data on  $\beta$  Pic have achieved a proper motion precision of  $0.02\text{--}0.03$  mas yr $^{-1}$  (Snellen & Brown 2018; Dupuy et al. 2019).

While this level of precision would be sufficient to measure the astrometric wobble of HD 100546, the  $\sim 24$  year time interval between the Hipparcos and Gaia mean epochs is close to the inferred 27-29 year orbital period of the companion, making it difficult to detect a wobble with the current Gaia DR2 data. To detect orbital acceleration we would need to measure a difference in the instantaneous proper motion of the star at two epochs.

For HD 100546, the difference between Gaia and the 24.5 year baseline is consistent with zero, ( $0.09 \pm 0.16$ ,  $0.02 \pm 0.14$ ) mas/yr, as expected for the inferred orbit, although with large errors. A better estimate will be available from the 5-year Gaia data and can be used to test for the presence of a supra-Jovian mass companion (T. Dupuy, private communication).

To summarize, we have presented ro-vibrational CO emission that is likely from the circumplanetary material orbiting a supra-Jovian mass companion in HD 100546. If confirmed, this will be the first direct detection of emitting gas from circumplanetary material. With more sensitive and higher resolution near and mid-infrared spectrographs on 30m class telescopes, we will be able to study the dynamics of the circumplanetary gas in more detail and measure the size of disk, determine whether the gas is in a Keplerian orbit, and thus better characterize the circumstellar disk - planet connection and the birthplace of Jovian moons.

We thank Trent Dupuy, Judit Szulagyi, Steph Sallum, and Thayne Currie for helpful discussion and advice. This work was performed in part at the Aspen Center for Physics which is supported by the National Science Foundation grant PHY-1607611. Work by SDB was performed in part at the National Optical Astronomy Observatory. NOAO is operated by the Association of Universities for Research in Astronomy (AURA), Inc. under a cooperative agreement with the National Science Foundation. SDB also acknowledges support from this work by NASA Agreement No. NXX15AD94G; NASA Agreement No. NNX16AJ81G; and NSF-AST 1517014.

## APPENDIX

An additional line of evidence pointing to the presence of a massive companion near the inner rim of the HD 100546 disk is the shape of the ro-vibrational OH emission line profile (Liskowsky et al. 2012; Brittain et al. 2014). The interaction between supra-Jovian mass planets and disks gives rise to a persistent eccentricity near the orbit of the planet (e.g., Kley & Dirksen 2006). Emission arising from an eccentric annulus has a distinct asymmetric line profile, similar to that observed from HD100546 (Liskowsky et al. 2012).

The result by Liskowsky et al. (2012) and Brittain et al. (2014) was called into question by Fedele et al. (2015). Fedele et al. (2015) compared several different observations of the OH line acquired at different epochs with different slit PAs and different line profiles. Because the equivalent width of one epoch with a relatively symmetric line profile is the largest, Fedele et al. (2015) conclude that this is the true shape of the OH line and that the previously reported asymmetries were spurious and caused by the occultation of the resolved disk by the relatively narrow slit.

Occulting a portion of the disk emission with a narrow slit can indeed give rise to an asymmetric line profile (e.g., Hein Bertelsen et al. 2014; Brittain et al. 2015; Fedele et al. 2015), although this explanation does not apply to our OH observations. Our spectra were taken in seeing-limited conditions and with a slit width large enough to encompass the entire inner rim. The diameter of the inner hole of HD 100546 is  $0''.29 \pm 0''.01$  (Jamialahmadi et al. 2018), whereas the slit was  $\sim 0''.4$ , and the seeing ranged from  $0''.6 - 0''.8$  (Liskowsky et al. 2012; Brittain et al. 2014, 2015). Both the seeing-limited nature of the observations and the large slit width relative to the inner rim limit the extent to which positioning offsets will affect the measured line profile.

In contrast, OH observations reported by Fedele et al. (2015) are much more likely to suffer from a spurious line profile produced by slit occultation. Their observations were made with a narrow slit width ( $0''.2$ ) that was very

closely matched to the PSF ( $0''.17$ ) and smaller than the diameter of the cleared region of HD 100546. Thus, it was impossible to avoid occulting some part of the inner rim at any position angle they observed. Additionally, slight offsets of the slit relative to the star could occult stellar light (or emission from the small ring of hot dust at  $\sim 2$  mas; Panić et al. 2014) relative to emission from the inner rim of the outer disk. As there is no significant NIR excess from the inner rim of the outer disk (Tatulli et al. 2011; Panić et al. 2014), such a scenario would give rise to a larger line to continuum ratio for the OH emission.

In contrast, our observations, which reveal an asymmetric OH emission profile, were taken without adaptive optics and with a slit that encompasses the entire inner rim. Furthermore, two observations with different instruments on different telescopes (Phoenix on Gemini South and CRRES on Gemini North) give the same line profile (Brittain et al. 2014). Observations of other transition disks with emission arising from the outer disk using a similar instrumental set up also do not reveal such line asymmetries (e.g., Brittain et al. 2007, 2009; Lewis et al. 2010; Brittain et al. 2018). Thus we conclude that the OH line profiles of HD 100546 are indeed intrinsically asymmetric and consistent with emission arising from an eccentric annulus.

## REFERENCES

- Ayliffe, B. A., & Bate, M. R. 2009, *MNRAS*, 397, 657
- Brittain, S. D., Carr, J. S., & Najita, J. R. 2018, *PASP*, 130, 074505
- Brittain, S. D., Carr, J. S., Najita, J. R., Quanz, S. P., & Meyer, M. R. 2014, *ApJ*, 791, 136
- Brittain, S. D., Najita, J. R., & Carr, J. S. 2009, *ApJ*, 702, 85
- . 2015, *Ap&SS*, 357, 54
- Brittain, S. D., Najita, J. R., Carr, J. S., et al. 2013, *ApJ*, 767, 159
- Brittain, S. D., Simon, T., Najita, J. R., & Rettig, T. W. 2007, *ApJ*, 659, 685
- Canup, R. M., & Ward, W. R. 2002, *AJ*, 124, 3404
- Carmona, A., van der Plas, G., van den Ancker, M. E., et al. 2011, *A&A*, 533, A39
- Casassus, S., & Perez, S. 2019, arXiv e-prints, arXiv:1906.06302
- Christiaens, V., Cantalloube, F., Casassus, S., et al. 2019, *ApJL*, 877, L33
- Close, L. M., Follette, K. B., Males, J. R., et al. 2014, *ApJL*, 781, L30
- Currie, T., Brittain, S., Grady, C. A., Kenyon, S. J., & Muto, T. 2017, *Research Notes of the American Astronomical Society*, 1, 40
- Currie, T., Cloutier, R., Brittain, S., et al. 2015, *ApJL*, 814, L27
- Dong, R., Najita, J. R., & Brittain, S. 2018, *ApJ*, 862, 103
- Dupuy, T. J., Brandt, T. D., Kratter, K. M., & Bowler, B. P. 2019, *ApJ*, 871, L4
- Fedele, D., Bruderer, S., van den Ancker, M. E., & Pascucci, I. 2015, *ApJ*, 800, 23
- Follette, K. B., Rameau, J., Dong, R., et al. 2017, *AJ*, 153, 264
- Gaia Collaboration, Brown, A. G. A., Vallenari, A., et al. 2018, *A&A*, 616, A1
- Gressel, O., Nelson, R. P., Turner, N. J., & Ziegler, U. 2013, *ApJ*, 779, 59
- Habart, E., Natta, A., Testi, L., & Carillet, M. 2006, *A&A*, 449, 1067
- Hein Bertelsen, R. P., Kamp, I., Goto, M., et al. 2014, *A&A*, 561, A102
- Hinkle, K. H., Cuberly, R. W., Gaughan, N. A., et al. 1998, in *Proc. SPIE*, Vol. 3354, *Infrared Astronomical Instrumentation*, ed. A. M. Fowler, 810–821
- Hinkle, K. H., Joyce, R. R., Sharp, N., & Valenti, J. A. 2000, in *Proc. SPIE*, Vol. 4008, *Optical and IR Telescope Instrumentation and Detectors*, ed. M. Iye & A. F. Moorwood, 720–728
- Hinkle, K. H., Blum, R. D., Joyce, R. R., et al. 2003, in *Proc. SPIE*, Vol. 4834, *Discoveries and Research Prospects from 6- to 10-Meter-Class Telescopes II*, ed. P. Guhathakurta, 353–363
- Jamialahmadi, N., Ratzka, T., Panić, O., et al. 2018, *ApJ*, 865, 137
- Kama, M., Folsom, C. P., & Pinilla, P. 2015, *A&A*, 582, L10
- Keppler, M., Benisty, M., Müller, A., et al. 2018, *A&A*, 617, A44
- Keppler, M., Teague, R., Bae, J., et al. 2019, arXiv e-prints, arXiv:1902.07639
- Klahr, H., & Kley, W. 2006, *A&A*, 445, 747
- Kley, W., & Dirksen, G. 2006, *A&A*, 447, 369
- Kraus, A. L., & Ireland, M. J. 2012, *ApJ*, 745, 5
- Kunde, V. R., & Maguire, W. C. 1974, *JQSRT*, 14, 803
- Lewis, J., Kronberg, M., & Brittain, S. 2010, *Journal of the Southeastern Association for Research in Astronomy*, 4, 20
- Liskowsky, J. P., Brittain, S. D., Najita, J. R., et al. 2012, *ApJ*, 760, 153
- Machida, M. N., Kokubo, E., Inutsuka, S.-I., & Matsumoto, T. 2010, *MNRAS*, 405, 1227

- Panić, O., Ratzka, T., Mulders, G. D., et al. 2014, *A&A*, 562, A101
- Pérez, S., Casassus, S., Hales, A., et al. 2019, arXiv e-prints, arXiv:1906.06305
- Pineda, J. E., Szulágyi, J., Quanz, S. P., et al. 2019, *ApJ*, 871, 48
- Pontoppidan, K. M., Blake, G. A., & Smette, A. 2011, *ApJ*, 733, 84
- Pontoppidan, K. M., Blake, G. A., van Dishoeck, E. F., et al. 2008, *ApJ*, 684, 1323
- Quillen, A. C., & Trilling, D. E. 1998, *ApJ*, 508, 707
- Rothman, L. S., Barbe, A., Benner, D. C., et al. 2003, *JQSRT*, 82, 5
- Sallum, S., Follette, K. B., Eisner, J. A., et al. 2015, *Nature*, 527, 342
- Snellen, I. A. G., & Brown, A. G. A. 2018, *Nature Astronomy*, 2, 883
- Szulágyi, J. 2017, *ApJ*, 842, 103
- Szulágyi, J., Morbidelli, A., Crida, A., & Masset, F. 2014, *ApJ*, 782, 65
- Szulágyi, J., & Mordasini, C. 2017, *MNRAS*, 465, L64
- Szulágyi, J., Plas, G. v. d., Meyer, M. R., et al. 2018, *MNRAS*, 473, 3573
- Tanigawa, T., Ohtsuki, K., & Machida, M. N. 2012, *ApJ*, 747, 47
- Tatulli, E., Benisty, M., Ménard, F., et al. 2011, *A&A*, 531, A1
- van der Plas, G., van den Ancker, M. E., Acke, B., et al. 2009, *A&A*, 500, 1137
- Wagner, K., Follette, K. B., Close, L. M., et al. 2018, *ApJL*, 863, L8
- Ward, W. R., & Canup, R. M. 2010, *AJ*, 140, 1168
- Waters, L. B. F. M., & Waelkens, C. 1998, *ARA&A*, 36, 233

**Table 1.** Journal of Observations

Date	Star	Int Time	Seeing	SNR
July 09, 2017	$\alpha$ Cru	8m	...	...
	HD 100546	88m	0''.9	120
December 03, 2017	HIP 60718	12m	...	...
	HD 100546	40m	1''.0	...
December 04, 2017	HIP 60718	12m	...	...
	HD 100546	64m	0''.8	130 <sup>a</sup>

<sup>a</sup>The signal-to-noise ratio of the combined data from December 3 and December 4.

**Table 2.** Hotband and  $^{13}\text{CO}$  lines

Isotopologue	$v''$	$J''$	$v'$	$J'$	$E''$	$\tilde{\nu}$	A
				$\text{cm}^{-1}$	$\text{cm}^{-1}$	$\text{s}^{-1}$	
$^{12}\text{CO}$	1	21	2	20	4103.67	2029.66	30.28
$^{12}\text{CO}$	2	15	3	14	5794.30	2030.16	45.75
$^{12}\text{CO}$	1	10	2	9	3353.92	2032.87	30.55
$^{12}\text{CO}$	3	8	4	7	7566.63	2033.14	62.96
$^{13}\text{CO}$	0	16	1	15	1557.06	2033.42	15.03
$^{12}\text{CO}$	2	14	3	13	5737.76	2034.41	46.15

NOTE—The hotband lines and the  $^{13}\text{CO}$  lines are excited by UV fluorescence (Brittain et al. 2009).

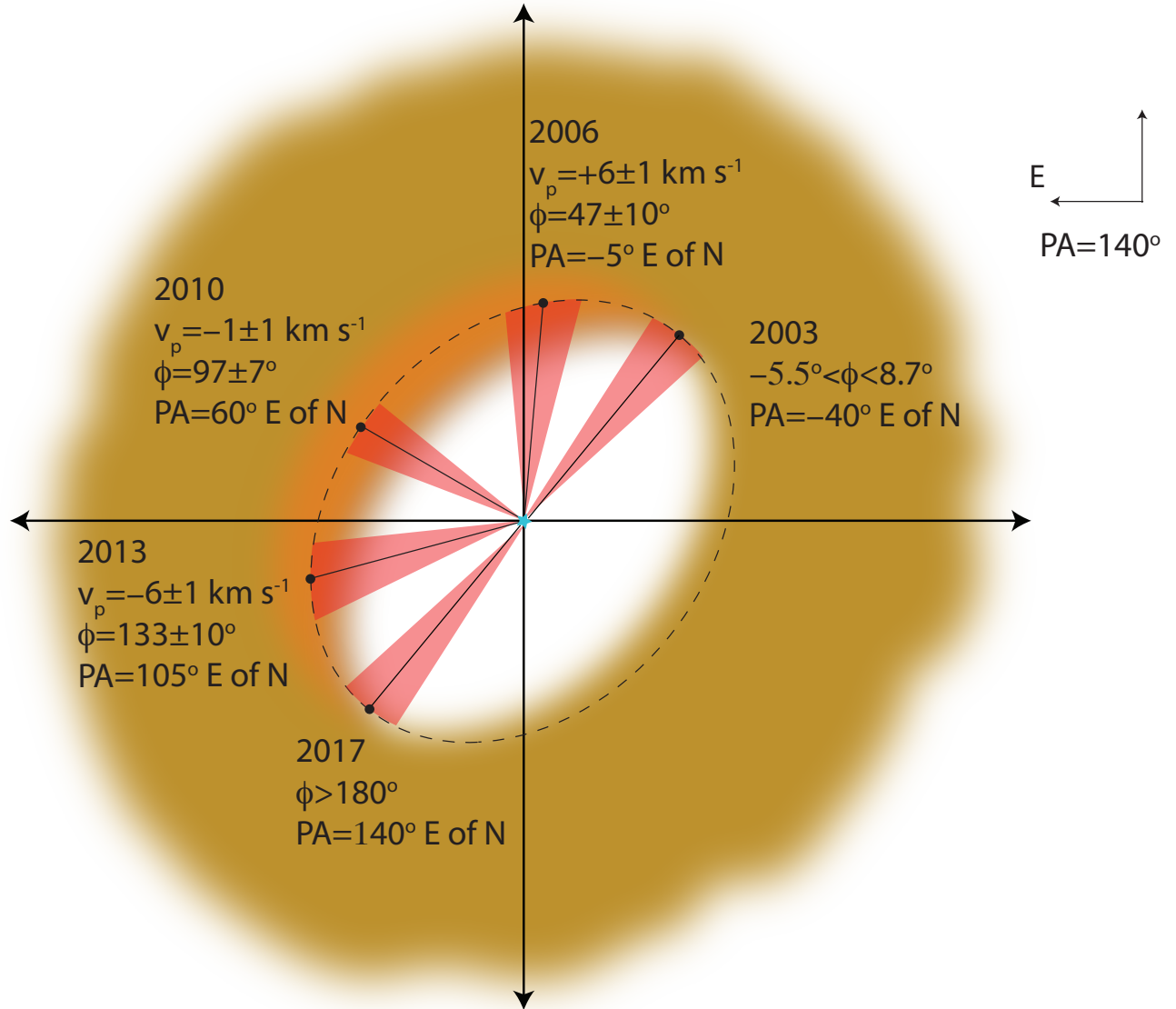


**Figure 1.** Schematic of the disk and orbiting source of excess CO emission identified in data taken from 2003 to 2017. The orbit is represented by the black dashed line. The disk wall of the disk is shaded orange. The location of the source of the emission excess is labeled with a black dot, and the uncertainty in the phase of the orbit is represented by the red sectors. We assume the excess CO emission is hidden by the near side of the circumstellar disk in 2003 and 2017.

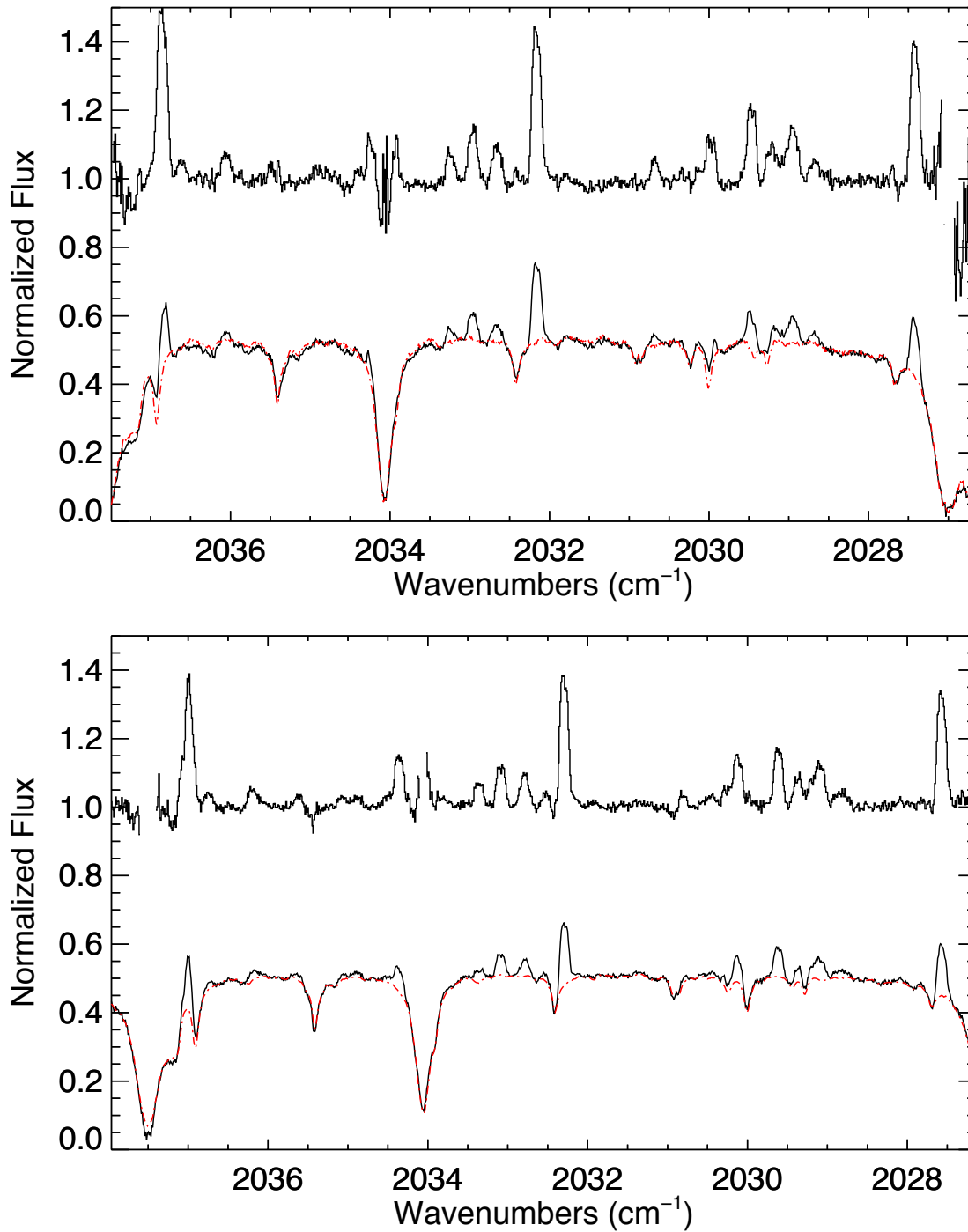


**Figure 2.** *M*-band spectrum of HD 100546 in July 2017 (upper panel) and December 2017 (lower panel). The spectrum of HD 100546 is plotted black with the telluric standard plotted in red. The ratioed spectrum is plotted above. Gaps in the spectra are regions where the atmospheric transmittance is less than 20%.

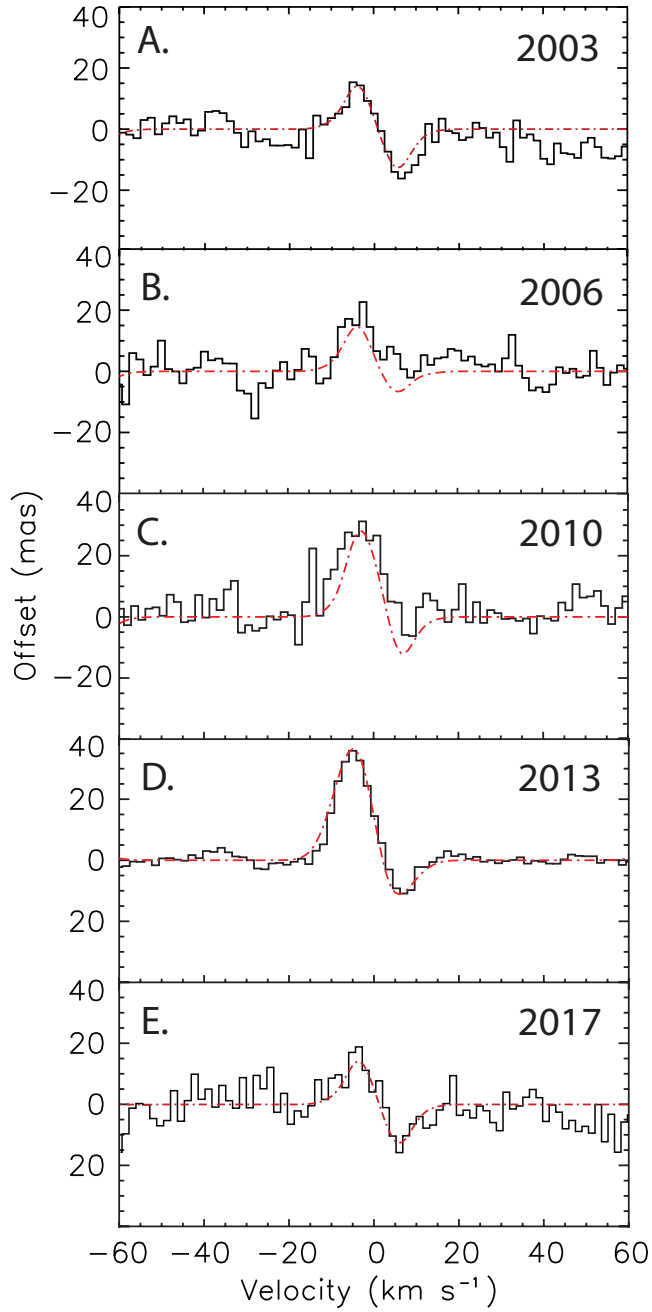


**Figure 3.** Spectroastrometric signal of the P26 line observed in each epoch (2003-2017). The spectroastrometric signal of the P26 line is detected in 2017 and consistent with gas in an axisymmetric, differentially rotating disk. It is also consistent with the signal observed in 2003. The asymmetry observed in previous epochs (2006 – 2013), due to the excess emission, is no longer observed.

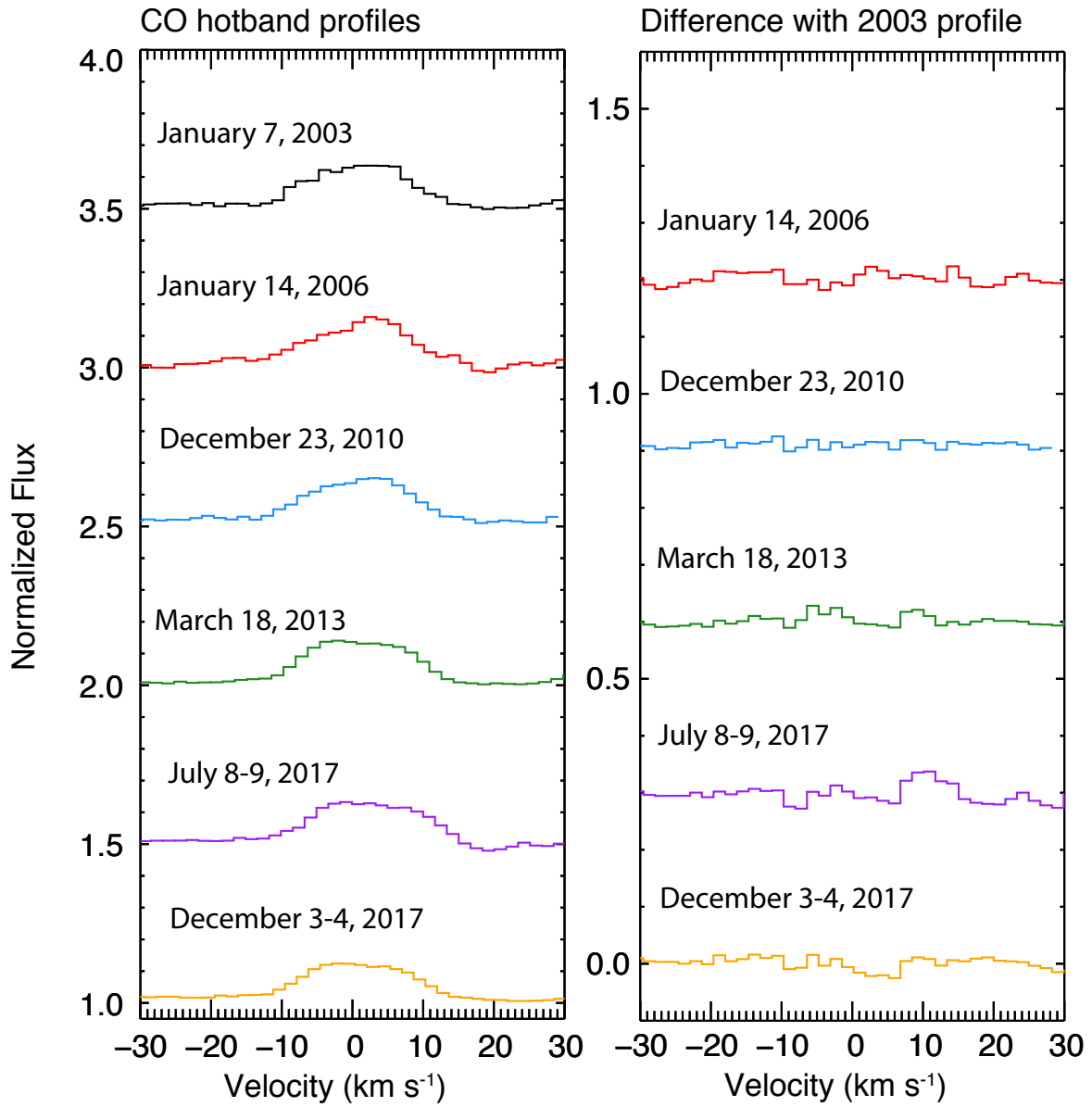


**Figure 4.** Multi-epoch observations of the average hotband line profile. Six hot band CO lines are averaged together and plotted for each date of observation (left panel). Each profile is differenced with the profile observed on January 7, 2003 (right panel). At the level of the S/N of the observations, there is no evidence of variability of the hotband CO lines.

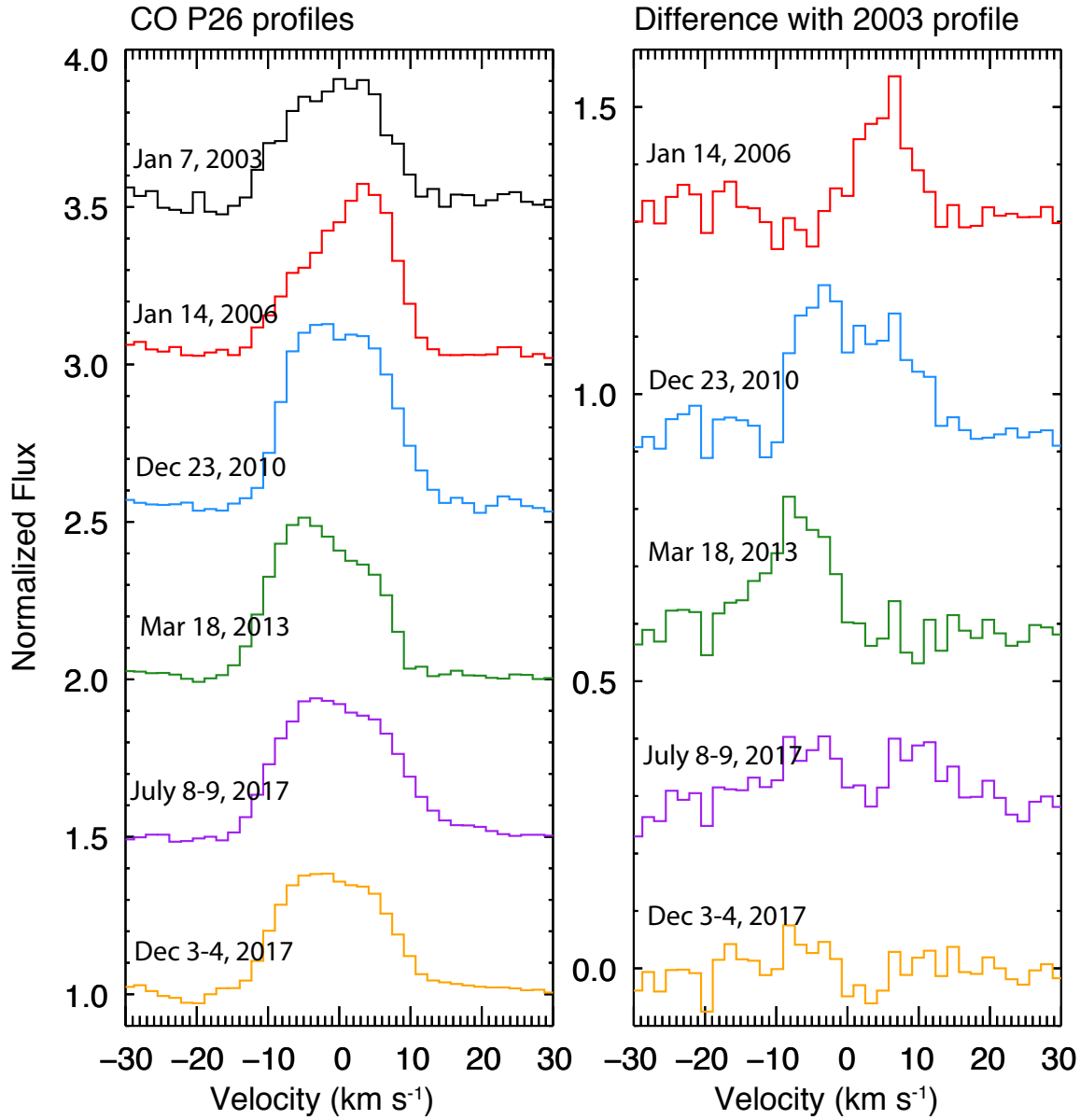


**Figure 5.** Multi-epoch observations of the  $v=1-0$  P26 line profile. The  $v=1-0$  P26 line is plotted over six epochs (left panel). Each profile is differenced with the profile observed on January 7, 2003 (right panel). Unlike the hot band lines, there is clear evidence of variability. The excess emission shifts from  $+6 \text{ km s}^{-1}$  on January 14, 2006 to  $-6 \text{ km s}^{-1}$  on March 18, 2013. By July 2017, the excess emission is gone.

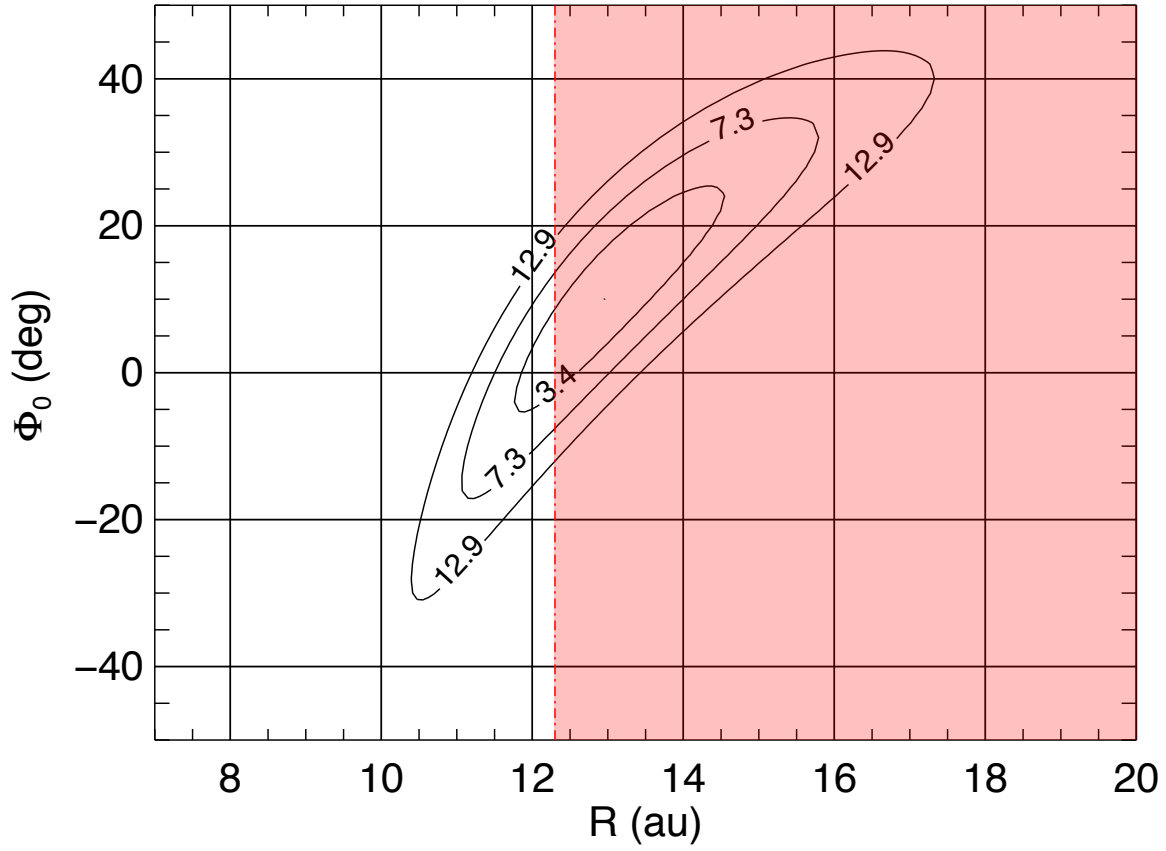


**Figure 6.** Constraint on the orbital radius  $R$  and orbital phase in 2003 ( $\phi_0$ ). The constraint is placed by fitting the projected velocities and relative phases in 2006, 2010, and 2013, assuming the excess CO emission is in a circular Keplerian orbit, the stellar mass is  $2.2M_{\odot}$ , and the inclination is  $47^{\circ}$ . The  $1\sigma$ ,  $2\sigma$ , and  $3\sigma$  confidence intervals are plotted. The disappearance of the emission by July 2017 indicates that the orbital period must be less than 29 years, thus we can rule out solutions with  $R > 12.3$  au (shaded region). Thus we find that  $11.6 < R < 12.3$  au and  $-5.5^{\circ} < \phi_0 < 8.7^{\circ}$ .